Electric Power Systems Research 214 (2023) 108819

Contents lists available at ScienceDirect

Electric Power Systems Research

journal homepage: www.elsevier.com/locate/epsr

A comprehensive strategy for the distribution network resilience enhancement considering the time-varying behaviors of typhoon path

Zhanghao Huang, Yachao Zhang *, Shiwei Xie

School of Electrical Engineering and Automation, Fuzhou University, Fuzhou City, Fujian Province, China

ARTICLE INFO

Keywords:
Typhoon events
Resilience-oriented scheduling framework
Spatially and temporally extended *N-k* uncertainty set
Nested column-and-constraint generation algorithm

ABSTRACT

Typhoon, as a high-impact and low-probability extreme event, can damage the components in power networks, thereby resulting in power outages or blackouts. To enhance the distribution network resilience against typhoon attacks, this paper proposes a resilience-oriented two-stage robust optimization model, in which resilience-constrained unit commitment schemes and planning-operational restoration measures are incorporated into a prevention and emergency response framework. In the prevention response stage, line hardening, flexible devices deployment, and unit commitment are performed before the typhoon attacks. During the typhoons, the emergency response is conducted to mitigate power outages by regulating soft open points, battery storage systems, and generation units. Moreover, considering the time-varying behaviors of typhoon path, the simulation technique for a sequential typhoon attack is developed to construct the spatially and temporally extended *N-k* uncertainty set for overhead line status. Thereafter, a tight approximation method is introduced to allow the proposed model to be a tractable mixed-integer linear programming problem, which can be easily solved by a nested column-and-constraint generation algorithm. Numerical results show that the comprehensive resilience-oriented strategies can respond rapidly to the worst-case scenario of typhoon attacks with cost-effective performance.

1. Introduction

Extreme weather events have adverse effects on the electrical power critical infrastructures, resulting in enormous economic losses and human casualties. For instance, between 2003 and 2012, weather-related outages affected more than 10 million people with an estimated $18-33 billion annual loss in the U.S. [1]. According to Ref. [2], recent hurricanes, such as Hurricane Irene and Typhoon Soudelor, struck the United States and China in 2011 and 2015 respectively, which led to widespread and devastating damages to power systems. Notably, the number and severity of these kinds of weather conditions have increased in recent years due to climate change [3]. Therefore, it is indispensable to recover the electric service effectively in response to a severe blackout induced by high-impact and low-probability events.

In particular, as the weaker part of the electricity grid, the distribution network (DN) is pretty vulnerable to extreme disasters, and thus promotes considerable research aiming to withstand and recover from severe disruptions [4]. Since power systems will undergo a multi-stage process when extreme weather occurs, the authors refer to the resilient DN that should be capable of anticipating, absorbing, adapting to, and recovering from outages [5]. In terms of the resilience improvement of the DN, planning actions are implemented for forthcoming catastrophes in the prevention response stage, while operational activities are coordinated during unfavorable disasters in the emergency response stage.

On the one hand, planning-oriented measures aim to protect the DN against natural catastrophes with different hardening strategies, such as vegetation management [6] and overhead line reinforcement [7]. Nevertheless, considering that hardening and upgrading the entire distribution system is considerably expensive, many types of research focus on the combination of various planning strategies. In [8], an optimal decision for line hardening and battery storage system (BSS) deployment is made to enhance the DN resilience. Likewise, the authors of [9] propose an integrated resilience framework, where the line hardening and distributed generation allocation are considered as the effective defense strategies against natural disasters. As a result, with an increasing type of resources in the modern power grid, how to cost-effectively design a resilient DN against the majority of dreadful attacks becomes a great challenge.

On the other hand, in the context of the active distribution system, resilience-based operation strategies containing a series of

* Corresponding author.
E-mail address: yczhang@fzu.edu.cn (Y. Zhang).

https://doi.org/10.1016/j.epsr.2022.108819
Received 3 April 2022; Received in revised form 27 August 2022; Accepted 15 September 2022
Available online 22 September 2022

Nomenclature

Abbreviations

DN	Distribution network
TN	Transmission network
GU	Generator unit
WT	Wind turbine
RO	Robust optimization
BSS	Battery storage system
SOP	Soft open point
SOC	Second order cone
RCUC	Resilience-constrained unit commitment
C&CG	Column-and-constraint generation
NC&CG	Nested column-and-constraint generation

Indices and Sets

t	Indices of time periods.
l_1,l_2	Indices of iteration for the NC&CG.
i,j,k	Indices for buses in the DN.
ij,jk	Indices for branches in the DN.
e,g,b,s(q)	Indices for the TN, GU, BSS, and SOP.
U_l	Multi-zone and multi-stage uncertainty set of line status.
Θ	Spatially and temporally extended N-k uncertainty set of line status
$\Omega_{N,t}, \Omega_{V,t}$	Sets of the normal and vulnerable lines.
$\Omega^{\mathrm{BR}}, \Omega^{\mathrm{DN}}$	Sets of branches and buses in the DN.
$\Omega^{\mathrm{GU}}, \Omega^{\mathrm{TN}}$	Sets of the buses connecting the GU and TN.
$\Omega^{\mathrm{BSS}}, \Omega^{\mathrm{SOP}}$	Sets of candidate locations for the BSS and SOP.
$\delta(j), \pi(j)$	Sets of the parent and child buses of bus j.

Parameters

$\Delta\rho_0$	Central pressure difference of the typhoon landing.
λ, v_0	The intrusion angle and moving speed of the typhoon.
σ, ξ	Empirical coefficient and Coriolis force parameter
$k_\varpi, N_{\varpi,\max}$	Number of vulnerable lines and all lines in Zone ϖ.
c^{L}	Hardening cost per unit length of the line.
l_{ij}	Length of line ij
c_t^{buy}	Electricity purchasing cost from the TN.
σ^{BSS}	Maximum discharge depth of the BSS.
ν^{BSS}	Energy level of the BSS at the initial time point.
$N^{\mathrm{L}}_{\max}, N^{\mathrm{BSS}}_{\max}$	Budget for hardening line and BSS installation.
$r_{\mathrm{S}}, r_{\mathrm{M}}$	Investment cost for the power/operation and maintenance of the SOP.
$\eta_{\mathrm{ch}}, \eta_{\mathrm{dis}}$	Charge/discharge efficiency of the BSS.
$a^{\mathrm{L}}, a^{\mathrm{BSS}}, a^{\mathrm{SOP}}$	Capital recovery factor of line hardening/BSS/SOP.
$k_{\mathrm{S}}, k_{\mathrm{E}}, k_{\mathrm{M}}$	Investment cost for the power/energy/operation and maintenance of the BSS.
c_g^{GU}	Fuel cost of the GU
$c_g^{\mathrm{on}}, c_g^{\mathrm{off}}$	Start-up and shut-down cost of the GU.
$c_g^{\mathrm{up}}, c_g^{\mathrm{down}}$	Upward and downward reserve cost of the GU.
$c_{\mathrm{sh}}, c^{\mathrm{GU}}_{g,\mathrm{cur}}$	Penalty cost of load shedding and power curtailment.
$c^{\mathrm{GU}}_{g,\mathrm{up}}, c^{\mathrm{GU}}_{g,\mathrm{down}}$	Upward/downward power regulation cost of the GU.
$T^{\mathrm{on}}_{g,\min}, T^{\mathrm{off}}_{g,\min}$	Minimum on and off time of the GU.
$U_{i,\min}, U_{i,\max}$	Minimum/maximum voltage of buses.
$P_{ij,\max}, Q_{ij,\max}$	Maximum active/reactive power of branches.
$P^{\mathrm{TN}}_{\max}, Q^{\mathrm{TN}}_{\max}$	Maximum active/reactive power from the TN.
$P^{\mathrm{Load}}_{i,t}, Q^{\mathrm{Load}}_{i,t}$	Load active/reactive power.
w_i	Weight coefficient of power load.
M	Large number for "Big-M" constraints
pf	Power factor of the GU.
U_0	Reference voltage magnitude.
r_{ij}, x_{ij}	Resistance/reactance of line ij.

Variables

r_t	Radius of wind field at time t.
$\Delta\rho_t, R_{\max,t}$	Central pressure difference and maximum wind speed radius at time t.
$v_{gx,t}, v_{\max,t}$	Maximum gradient wind speed and maximum wind speed at time t.
$Q^{\mathrm{BSS}}_{b,t}$	Reactive power of the BSS at time t.
$S^{\mathrm{BSS}}_b, E^{\mathrm{BSS}}_b$	Power/energy capacity of the BSS.
$\beta^{\mathrm{BSS}}_{b,t,\mathrm{ch}}, \beta^{\mathrm{BSS}}_{b,t,\mathrm{dis}}$	Charge/discharge status of the BSS at time t.
$P^{\mathrm{BSS}}_{b,t,\mathrm{ch}}, P^{\mathrm{BSS}}_{b,t,\mathrm{dis}}$	Charge/discharge power of the BSS at time t.
S^{SOP}_s	Power capacity of the SOP.
$P^{\mathrm{SOP}}_{s,t}, Q^{\mathrm{SOP}}_{s,t}$	Active and reactive power of the SOP at time t.
$Q^{\mathrm{GU}}_{g,t,\max}$	Maximum reactive power of the GU at time t.
$\Delta Q^{\mathrm{GU}}_{g,t}$	Reactive power adjustment of the GU at time t.
$P^{\mathrm{GU}}_{g,t,\mathrm{cur}}$	Active power curtailment of the GU at time t.
$P^{\mathrm{GU}}_{g,t,\mathrm{up}}, P^{\mathrm{GU}}_{g,t,\mathrm{down}}$	Upward/downward power regulation of the GU at time t.
$P^{\mathrm{GU}}_{g,t}, Q^{\mathrm{GU}}_{g,t}$	Active/reactive power output of the GU at time t.
$D^{\mathrm{up}}_{g,t}, D^{\mathrm{down}}_{g,t}$	Upward/downward reserve capacity of the GU at time t.
$P^{\mathrm{TN}}_{h,t}, Q^{\mathrm{TN}}_{h,t}$	Active and reactive power of the TN at time t.
$P^{\mathrm{Load}}_{i,t,\mathrm{sh}}, Q^{\mathrm{Load}}_{i,t,\mathrm{sh}}$	Active/reactive load shedding for bus i at time t.
$P_{i,t}, Q_{i,t}$	Total active/reactive power injection for bus i at time t.
$P_{ij,t}, Q_{ij,t}$	Active/reactive power flow from bus i to j at time t.
$U_{i,t}$	Voltage for bus i at time t.
$\Pr(ij,t)$	Failure probability of branch ij at time t.
$u_{ij,t}$	Binary variables for line attack: 0 if line ij is attacked at time t; 1 otherwise.
h_{ij}	Binary variables for line hardening: 1 if line ij is hardened; 0 otherwise.
$\theta_{ij,t}$	Binary variables for line status: 1 if line ij is normal at time t; 0 otherwise.
α_i	Binary variables for the BSS installation: 1 if the BSS is installed at bus i; 0 otherwise.
$\chi_{i,t}$	Binary variables for startup state of the GU: 1 if the GU starts up at time t; 0 otherwise.
$\gamma_{i,t}$	Binary variables for shutdown state of the GU: 1 if the GU shuts down at time t; 0 otherwise.
$\delta_{i,t}$	Binary variables for on/off state of the GU: 1 if the GU is running at time t; 0 otherwise.

interdependent control actions can coordinate multiple controllable resources over a time horizon [10]. So far, some studies have delved into combinational operation activities to achieve high resilience in the DN. In [8], the transfer power supply and BSS are coordinated to ensure the continual power supply for critical loads. However, the BSS is only used as a power supply without considering its charging feature that is conducive to safe and stable operation for power systems during extreme events. In [11], the topology switching and generator re-dispatch are integrated into a resilience response framework, aiming to enhance the resilience adaptation ability of power grids. It is noticeable that the tie switch movement may need some time to complete so that power outages could be last for several hours. As an alternation to achieve load recovery, the soft open point (SOP) can not only provide active power flow control and reactive power compensation, but also quickly isolate

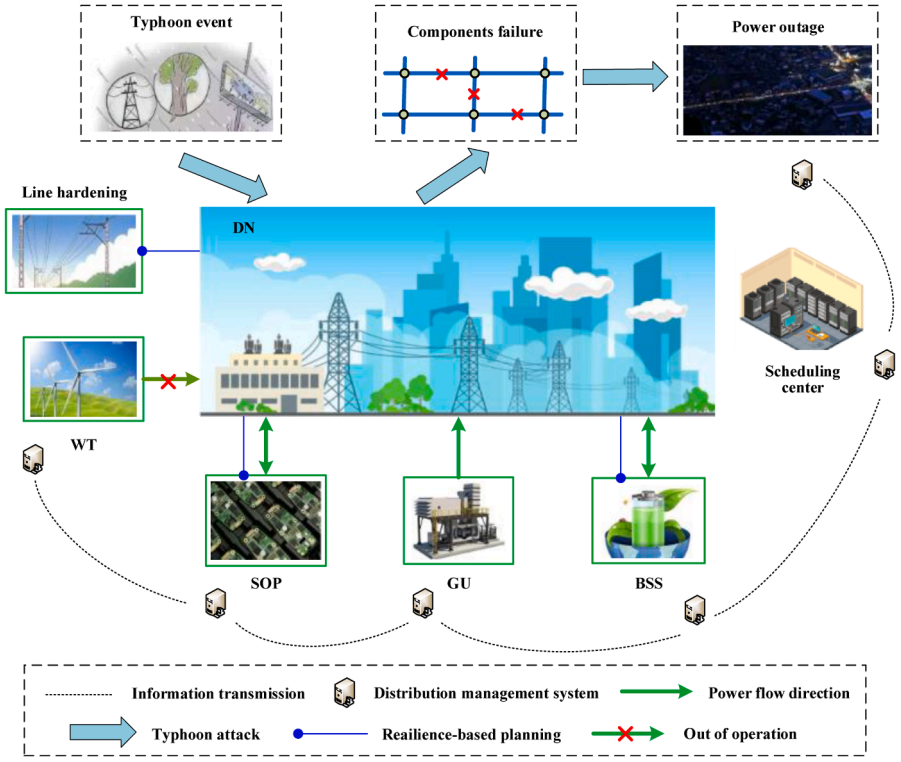

Fig. 1. Schematic diagram of the resilient DN.

the extreme condition faults and provide effective voltage support when a contingency event occurs [12].

In addition to some electronic devices, some scholars refer to the studies of an optimal resilience-constrained unit commitment (RCUC) in case of imminent extreme weather. In [13], an RCUC model is developed to adjust pre-contingency generation schedules and give a guidance for market players in advance. References [14] and [15] formulate the day-ahead unit commitment framework to enhance the power system resilience against extreme weather events. Notably, the above studies only focus on modeling of *N-k* unit commitment rather than other equipment that could reduce the risk of generation curtailment. Since there exist multiple electronic device and distributed generators with fast response capability in the DN, it is necessary to formulate an RCUC strategy with a small time-scale for the DN against extreme events. For instance, the turboshaft gas turbine unit of General Electric LM6000 can reach its maximum power in 5 minutes reported in [16]. In addition, the charge-discharge status of the BSS is often determined before extreme events as the here-and-now decision in [8,17] and [18], which can be considered as the wait-and-see decision for the resilience improvement of the DN during the incident.

It is critical to take into account the uncertainties of system components outage before making the proactive decision against the natural disasters. To this end, many studies focus on stochastic programming [19–21] and robust optimization (RO) [22–24] methods to model the impact of natural disasters on the power system. In [19], to address the uncertainties of fault locations, Monte Carlo Simulation is employed to generate 10000 scenarios considering different type, severity level and location of the incident. However, the stochastic programming problem could become difficult to solve as the number of credible contingencies increases. In [24], a two-stage robust optimization framework is developed for the classic defense-attack-defense model, where the sequential characteristics of typhoon attacks are not taken into account. Since typhoons often have a time-varying track and intensity, the towers and conductors in the power network could be destroyed along with the evolution of typhoons [25]. In the light of the continuous time-changing weather conditions of typhoons, considerable efforts have been devoted to modeling the spatiotemporal feature of component outage in power systems, i.e., the Markov property [26]. Reference [21] proposes a stochastic model for possible typhoon paths, where power lines in each typhoon path are on outage within a certain probability. In [27], a multi-state and regional weather model is developed for power system reliability under hurricanes. Furthermore, a multi-zone and multi-stage uncertainty set is constructed to capture the spatiotemporal dynamic characteristics of windstorms' impact on electrical components [28]. From the above analysis, a reliable method to evaluate the impact of typhoons on power systems plays an important role in the defender's decision-making process.

In this paper, to improve the DN resilience, a resilience-oriented two-stage robust optimization (RO) model with a comprehensive planning-operation framework is proposed. The main contributions are summarized as follows:

1) **A comprehensive planning-operation framework including the RCUC is tailored for the resilient DN.** In the previous studies [13–15], the resilient unit commitment is decided on an hourly scale and the advantage of electronic devices is not considered therein, putting the generation units at the risk of generation curtailment due to the physical limit. To improve the DN resilience, minute-level RCUC schemes and planning-operational defensive measures are integrated into a comprehensive planning-operation framework.
2) **A spatially and temporally extended *N-k* uncertainty set of the vulnerable lines is constructed.** Although the multi-zone and multi-stage uncertainty set has been reported in the existing literature [8,25,28], it is not built based on the simulation of the typhoon path evolution. In this study, we use the Batts typhoon model to characterize the time-varying behaviors of the typhoon path. On this basis, the view of square mesh grids is adopted to obtain the wind speeds that determine the spatially and temporally extended *N-k* uncertainty set of line status. Moreover, the Monte Carlo simulation

is properly designed to search for the worst-case contingency caused by typhoons.

3) **A resilience-oriented two-stage robust optimization model for the DN is presented.** Instead of committing BSS in the first stage (here-and-now) of the decision-making process, the proposed model optimizes the charge-discharge status of BSS as the second-stage (wait-and-see) decisions. In this way, the BSS can respond quickly to the emergency events unfolding and thus provide more flexibility for the DN to deal with typhoon-caused contingencies. Subsequently, a tight approximation method is introduced to allow the proposed model to be a tractable linear programming problem, which can be solved by a nested column-and-constraint generation (NC&CG) algorithm.

The remainder of the paper is organized as follows: the framework of the resilient DN is described in Section 2. A spatially and temporally extended *N-k* uncertainty set of the vulnerable lines is constructed in Section 3. In Section 4, the mathematical formulation of the resilience-oriented two-stage robust optimization model is presented. Section 5 introduces the solution methodology for the resilience-oriented model. Section 6 illustrates the case studies. The conclusions are given in Section 7.

2. The framework of the resilient DN

Modern DNs have been furnished with the massive proliferation of advanced smart grid technologies, e.g., distribution management system, distributed energy resources (e.g., wind turbines), the SOP, and the BSS, providing operational flexibility that can be harnessed for resilience improvement during emergencies. Notably, since the cut-out wind speed for a wind turbine (WT) is far less than the maximum sustained wind speed of the typhoon, the WT often should be out of operation to avoid being damaged when the typhoon occurs [29]. In this context, the framework of resilient DN is presented as shown in Fig. 1. In the face of typhoons, overhead lines could be brought down because of bending trees or fragile poles caused by high winds [30], which is a sequential process modeled by a spatially and temporally extended *N-k* uncertainty set of power lines' status. As a result, the electricity supplied to consumers would be interrupted. To address this problem, the line hardening and the dispatch of SOP, GU, and BSS are regarded as a coordinated planning-operation strategy to enhance the DN resilience, which is made by operators in the scheduling center of the distribution management system.

3. State modeling of the line attacked by typhoons

3.1. Typhoon simulation model

The Batts typhoon model, as one of the most mature wind field models, is adopted to simulate a specific typhoon event [21]. As shown in Fig. 2, the direction, range, and intensity of a typhoon are leveraged to estimate the typhoon track passing through the DN. Furthermore, the track area is divided into a certain number of mesh cells of a few square kilometers, where the wind speed is assumed to be the same as that at the central location, e.g. pink squares A and B in Fig. 2. Based on the Batts typhoon model, the wind speed of the typhoon can be calculated as follows:

$$\Delta\rho_t = \Delta\rho_0 - 0.675(1+\sin\lambda)t, \forall t \tag{1}$$

$$R_{\max,t} = \exp\left(-0.1239\Delta\rho_t^{0.6003} + 5.1043\right), \forall t \tag{2}$$

$$v_{gx,t} = \sigma\sqrt{\Delta\rho_t} - 0.5R_{\max,t}\xi, \forall t \tag{3}$$

$$v_{\max,t} = 0.865v_{gx,t} + 0.5v_0, \forall t \tag{4}$$

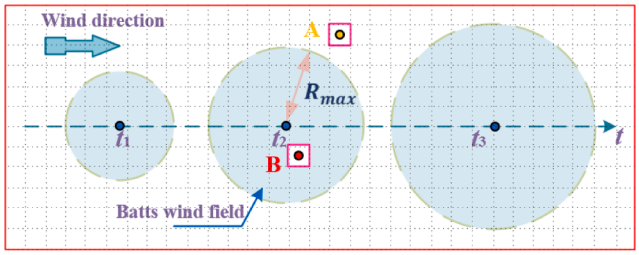

Fig. 2. Schematic diagram of typhoon landing process.

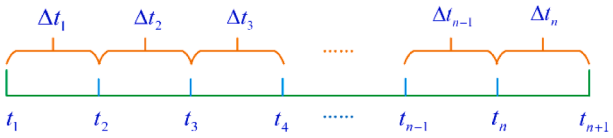

Fig. 3. Sequential process of the typhoon attacks.

$$v_t = \begin{cases} \dfrac{v_{\max,t}r_t}{R_{\max,t}}, r_t \le R_{\max,t} \\ v_{\max,t}\left(\dfrac{R_{\max,t}}{r_t}\right)^{\vartheta}, r_t > R_{\max,t} \end{cases}, \forall t \tag{5}$$

where Eq. (1) presents that the central pressure difference of the typhoon decays over time after the typhoon makes landfall. Expression (2) describes the relationship between the radius of maximum wind speed and the central pressure difference. Eq. (3) denotes the maximum gradient wind speed is caused by pressure gradient force. Eq. (4) indicates that the maximum wind speed is determined by the maximum gradient wind speed and the moving speed of the typhoon center. Expression (5) gives the wind speed at any location of the typhoon wind field. ϑ is a constant in the range of 0.5 to 0.7. [21].

In practice, the typhoon attack on the distribution network is a sequential process that can be characterized by wind speeds. For clarity, it is assumed that the entire process is divided into n periods as shown in Fig. 3. During the nth period (t_n~t_{n+1}), the corresponding wind speed is given as follows:

$$v_{\Delta t_n} = \frac{1}{\Delta t_n}\int_{t_n}^{t_{n+1}} v_t \mathrm{d}t \tag{6}$$

In terms of the mesh view of the power grid, the transmission line may span more than one mesh cell due to its long size. In the DN, the line is usually composed of overhead conductors and distribution poles in series [21]. Therefore, it is assumed that the conductor segments and poles in each mesh cell fail independently. When at least one of conductor segments or poles fails, the line is considered to fail. On this basis, the wind speed by (6) is mapped to the fragility curves of conductors and poles to derive the failure probability of overhead lines as follows [31,32]:

$$\mathrm{Pr}_n(ij,t) = 1 - \prod_{c}^{C_n}[1 - Pr_c(t)]\prod_{p}^{P_n}[1 - Pr_p(t)], \forall ij \in \Omega^{\mathrm{BR}}, \forall t \tag{7}$$

$$\mathrm{Pr}(ij,t) = 1 - \prod_{n=1}^{N}[1 - \mathrm{Pr}_n(ij,t)], \forall ij \in \Omega^{\mathrm{BR}}, \forall t \tag{8}$$

To trade off the operation cost and the decision conservativeness, the vulnerability threshold $\mathrm{Pr}_{V,th}$ is regarded as a criterion to determine the vulnerable lines. If the failure probability $\mathrm{Pr}(ij,t)$ exceeds the threshold, the line is vulnerable.

$$\begin{cases} ij \in \Omega_{N,t}, \text{if} \mathrm{Pr}(ij,t) < \mathrm{Pr}_{V,th}, \forall ij \in \Omega^{\mathrm{BR}}, \forall t \\ ij \in \Omega_{V,t}, \text{if} \mathrm{Pr}(ij,t) \ge \mathrm{Pr}_{V,th}, \forall ij \in \Omega^{\mathrm{BR}}, \forall t \end{cases} \tag{9}$$

3.2. The uncertainty set of vulnerable lines

Considering the temporal and spatial influence of typhoons on the DN, we put the operation status of all lines into the three stages that are normal stage, destruction stage, and degraded stage, respectively. For notion brevity, we firstly assume that the typhoon sequentially passes through the zone $\Omega_1, \Omega_2, \cdots, \Omega_\varsigma$ with time series $t_1, t_2, \cdots, t_\varsigma$. Then, a multi-zone and multi-stage uncertainty set is developed to deal with the uncertainties of the line status. In each zone, the number of vulnerable lines determined by (9) conforms with the $N-k$ criterion, which can be used to estimate the impact of the typhoon on the DN.

1) Normal stage

Before the typhoon attacks at the period t_0, the lines in all zones ($\Omega_1, \Omega_2, \ldots, \Omega_\varsigma$) keep the normal operation without outage risk. Consequently, the line status set in the zones can be presented as:

$$U_l^{No} = \{u_{ij,t} | u_{ij,t} = 1, \forall ij \in \{\Omega_1, \Omega_2, \cdots, \Omega_\varsigma\}, \forall t \in t_0\} \tag{10}$$

2) Disruption stage

Since the Ω_1 is attacked firstly by the typhoon, the corresponding line status at the period t_1 may change from "1" to "0". For the other unaffected zones $\{\Omega / \Omega_1\}$, the line status is the same as that at the previous periods. When the typhoon attacks the zones $\Omega_2, \Omega_3, \ldots, \Omega_\varsigma$ in turn, all areas of the DN are affected until time period t_ς. As a result, the line status set in the disruption stage can be expressed as follows:

$$\left.\begin{aligned} U_l^{Di} = \Bigg\{ u_{ij,t} \Bigg| & \sum_{ij \in \Omega_1} (1 - u_{ij,t}) \le N_{1,\max}, \forall t \in t_1 \\ & u_{ij,t_1} = u_{ij,t_0}, \forall ij \in \{\Omega / \Omega_1\}, \\ & \sum_{ij \in \Omega_2} (1 - u_{ij,t}) \le N_{2,\max}, \forall t \in t_2 \\ & u_{ij,t_2} = u_{ij,t_1}, \forall ij \in \{\Omega / \Omega_2\}, \\ & \vdots \\ & \sum_{ij \in \Omega_\varsigma} (1 - u_{ij,t}) \le N_{\varsigma,\max}, \forall t \in t_\varsigma \\ & u_{ij,t_\varsigma} = u_{ij,t_{\varsigma-1}}, \forall ij \in \{\Omega / \Omega_\varsigma\} \end{aligned} \Bigg\}\right. \tag{11}$$

3) Degraded stage

After all zones are attacked, the DN will be degraded at the period $t_{\varsigma+1}$. The line status in each zone should be the same as that in the disruption stage, which can be indicated as

$$U_l^{De} = \left\{ u_{ij,t} \middle| u_{ij,t} = u_{ij,t_\varsigma}, \forall ij \in \{\Omega_1, \Omega_2, \cdots, \Omega_\varsigma\}, \forall t \in t_{\varsigma+1} \right\} \tag{12}$$

To describe the line status of the DN before, during, and after the typhoon, the above uncertainty sets are combined into the multi-zone and multi-stage uncertainty set as follows:

$$U_l = U_l^{No} \cup U_l^{Di} \cup U_l^{De} \tag{13}$$

In fact, the operation status of a distribution line is determined by the hardening decision and the typhoon attack [33]. When a line is reinforced, we consider that the line cannot be damaged although it is attacked by the typhoon. Furthermore, given that typhoons occur in a less frequent fashion, the *N-k* criterion is adopted to limit the contingencies of line failure. As a result, the spatially and temporally extended *N-k* uncertainty set of line status is expressed as follows:

$$\Theta = \left\{ \theta_{ij,t} \middle| \begin{aligned} & \theta_{ij,t} = 1 - (1 - h_{ij})(1 - u_{ij,t}), \forall ij \in \Omega^{\mathrm{BR}}, \forall t \\ & \sum_{ij \in \Omega_\varpi} \theta_{ij,t} \ge N_{\varpi,max} - k_\varpi, \forall \varpi \in \{1, 2, \cdots \varsigma\}, \forall t \end{aligned} \right\} \tag{14}$$

To facilitate the solution, the multiplication of two binary variables in (14) can be linearized as:

$$\begin{cases} \theta_{ij,t} \ge h_{ij}, \theta_{ij,t} \ge u_{ij,t} \\ \theta_{ij,t} \le h_{ij} + u_{ij,t} \end{cases}, \forall ij \in \Omega^{\mathrm{BR}}, \forall t \tag{15}$$

4. The resilience-oriented two-stage model

In this section, a resilience-oriented two-stage model is developed for the DN, where the resilience-constrained unit commitment and planning-operational restoration measures are incorporated into the framework of prevention and emergency responses. As a result, the planning decisions, consisting of the line hardening strategy, the pre-dispatch of the GU, and the deployment of the BSS and SOP, are determined in the prevention response stage before typhoon attacks. During the typhoon event, the real-time scheduling of the GU, BSS, and SOP can be implemented in the emergency response stage.

4.1. Prevention response stage

In the prevention stage, the line hardening and the capacity configuration of the BSS and SOP are considered as the planning decisions, the total investment costs for which can be presented as follows:

$$C_1^{\mathrm{Plan}} = C^{\mathrm{L}} + C^{\mathrm{BSS}} + C^{\mathrm{SOP}} \tag{16}$$

$$C^{\mathrm{L}} = a^{\mathrm{L}} \sum_{ij \in \Omega^{\mathrm{BR}}} h_{ij} c^{\mathrm{L}} l_{ij} \tag{17}$$

$$\begin{cases} C_{\mathrm{inv}}^{\mathrm{BSS}} = \sum_{b \in \Omega^{\mathrm{BSS}}} \left(k_{\mathrm{S}} S_b^{\mathrm{BSS}} + k_{\mathrm{E}} E_b^{\mathrm{BSS}} \right) \\ C_{\mathrm{on}}^{\mathrm{BSS}} = \sum_{b \in \Omega^{\mathrm{BSS}}} k_{\mathrm{S}} k_{\mathrm{M}} S_b^{\mathrm{BSS}} \\ C^{\mathrm{BSS}} = \left(a^{\mathrm{BSS}} C_{\mathrm{inv}}^{\mathrm{BSS}} + C_{\mathrm{on}}^{\mathrm{BSS}} \right) \end{cases} \tag{18}$$

$$\begin{cases} C_{\mathrm{inv}}^{\mathrm{SOP}} = \sum_{s \in \Omega^{\mathrm{SOP}}} r_{\mathrm{S}} S_s^{\mathrm{SOP}} \\ C_{\mathrm{on}}^{\mathrm{SOP}} = \sum_{s \in \Omega^{\mathrm{SOP}}} r_{\mathrm{S}} r_{\mathrm{M}} S_s^{\mathrm{SOP}} \\ C^{\mathrm{SOP}} = \left(a^{\mathrm{SOP}} C_{\mathrm{inv}}^{\mathrm{SOP}} + C_{\mathrm{on}}^{\mathrm{SOP}} \right) \end{cases} \tag{19}$$

$$a = \frac{\tau (1 + \tau)^y}{(1 + \tau)^y - 1}, a \in \left\{ a^{\mathrm{BSS}}, a^{\mathrm{SOP}} \right\} \tag{20}$$

$$\begin{cases} 0 \le S_b^{\mathrm{BSS}} \le \alpha_b S_{b,\max}^{\mathrm{BSS}} \\ 0 \le E_b^{\mathrm{BSS}} \le \alpha_b E_{b,\max}^{\mathrm{BSS}} \end{cases}, \forall b \in \Omega^{\mathrm{BSS}} \tag{21}$$

$$0 \le S_s^{\mathrm{SOP}} \le S_{s,\max}^{\mathrm{SOP}}, \forall s \in \Omega^{\mathrm{SOP}} \tag{22}$$

$$\sum_{b \in \Omega^{\mathrm{BSS}}} \alpha_b \le N_{\max}^{\mathrm{BSS}} \tag{23}$$

$$\sum_{ij \in \Omega^{\mathrm{BR}}} h_{ij} \le N_{l,\max} \tag{24}$$

where Eq. (16) denotes the total planning costs. Eq. (17) represents the cost of line hardening. Eqs. (18) and (19) denote the total deployment costs for the BSS and SOP, which include equipment investment cost as well as operation and maintenance expenses, respectively. Eq. (20) gives the capital recovery factor of the BSS and SOP deployment. Constraints (21) and (22) impose capacity limits on the BSS and SOP, respectively. Constraint (23) limits the maximum number of the installed BSS. Constraint (24) gives a maximum budget of hardened lines.

According to the typhoon information from the meteorological department in advance, the power output and spinning reserve of the GUs are determined in the pre-contingency stage as follows:

$$C_{\mathrm{I}}^{\mathrm{GU}}=\sum_{g\in\Omega^{\mathrm{GU}}}\sum_{t\in T}\begin{pmatrix}c_g^{\mathrm{GU}}P_{g,t}^{\mathrm{GU}}+c_g^{\mathrm{on}}\chi_{g,t}+c_g^{\mathrm{off}}\gamma_{g,t}\\+c_g^{up}D_{g,t}^{up}+c_g^{down}D_{g,t}^{down}\end{pmatrix} \tag{25}$$

$$\delta_{g,t}P_{i,\min}^{\mathrm{GU}}\le P_{g,t}^{\mathrm{GU}}\le\delta_{g,t}P_{g,\max}^{\mathrm{GU}},\forall g\in\Omega^{\mathrm{GU}},\forall t \tag{26}$$

$$Q_{g,t,\max}^{\mathrm{GU}}=P_{g,t}^{\mathrm{GU}}\tan\left(\cos^{-1}(\mathrm{pf}_1)\right),\forall g\in\Omega^{\mathrm{GU}},\forall t \tag{27}$$

$$-Q_{g,t,\max}^{\mathrm{GU}}\le Q_{g,t}^{\mathrm{GU}}\le Q_{g,t,\max}^{\mathrm{GU}},\forall g\in\Omega^{\mathrm{GU}},\forall t \tag{28}$$

$$P_{g,t}^{\mathrm{GU}}-P_{g,t-1}^{\mathrm{GU}}\le R_g^{up},\forall g\in\Omega^{\mathrm{GU}},\forall t \tag{29}$$

$$P_{g,t-1}^{\mathrm{GU}}-P_{g,t}^{\mathrm{GU}}\le R_g^{down},\forall g\in\Omega^{\mathrm{GU}},\forall t \tag{30}$$

$$0\le D_{g,t}^{up}\le\left(\delta_{g,t}P_{g,\max}^{\mathrm{GU}}-P_{g,t}^{\mathrm{GU}}\right),\forall g\in\Omega^{\mathrm{GU}},\forall t \tag{31}$$

$$0\le D_{g,t}^{down}\le\left(P_{g,t}^{\mathrm{GU}}-\delta_{g,t}P_{g,\min}^{\mathrm{GU}}\right),\forall g\in\Omega^{\mathrm{GU}},\forall t \tag{32}$$

$$\left(t_{g,t-1}^{\mathrm{on}}-T_{g,\min}^{\mathrm{on}}\right)\left(\delta_{g,t-1}-\delta_{g,t}\right)\ge 0,\forall g\in\Omega^{\mathrm{GU}},\forall t \tag{33}$$

$$\left(t_{g,t-1}^{\mathrm{off}}-T_{g,\min}^{\mathrm{off}}\right)\left(\delta_{g,t}-\delta_{g,t-1}\right)\ge 0,\forall g\in\Omega^{\mathrm{GU}},\forall t \tag{34}$$

$$\begin{cases}\chi_{g,t}-\gamma_{g,t}=\delta_{g,t}-\delta_{g,t-1}\\ \chi_{g,t}+\gamma_{g,t}\le 1\end{cases},\forall g\in\Omega^{\mathrm{GU}},\forall t \tag{35}$$

where Eq. (25) denotes the preventive scheduling cost of the GUs, including the costs of power generation, start-up, shut-down, and spinning reserve. Constraints (26)-(28) limit the active and reactive power outputs of the GUs, in which the maximum reactive power of the GUs is determined by the power factor and active power output. Constraints (29) and (30) denote the ramp up and down limits of the GUs. Constraints (31) and (32) determine the reserve capacity of the GUs. Constraints (33) and (34) specify the minimum on/off time duration of each unit. Constraint (35) describes the relationship between the start-up/shut-down process and the unit state.

4.2. Emergency response stage

In the emergency response stage, the power supply from the transmission network (TN), the GUs re-dispatch, and the electronic device operation are integrated into an emergency response framework to defend against typhoon attacks. Accordingly, the objective function (36) aims to minimize the costs of power purchasing, load shedding, generation curtailment, and generation adjustment, while respecting the system operation constraints (37)-(68).

$$C_{\mathrm{II}}^{\mathrm{Op}}=\sum_{t\in T}\begin{pmatrix}\sum_{e\in\Omega^{\mathrm{TN}}}c_t^{\mathrm{buy}}P_{e,t}^{\mathrm{TN}}+c_{\mathrm{sh}}\sum_{i\in\Omega^{\mathrm{DN}}}w_iP_{i,t,\mathrm{sh}}^{\mathrm{Load}}+\sum_{g\in\Omega^{\mathrm{GU}}}c_{g,\mathrm{cur}}^{GU}P_{g,t,\mathrm{cur}}^{\mathrm{GU}}\\+\sum_{g\in\Omega^{\mathrm{GU}}}c_{g,up}^{\mathrm{GU}}P_{g,t,up}^{\mathrm{GU}}+\sum_{g\in\Omega^{\mathrm{GU}}}c_{g,down}^{\mathrm{GU}}P_{g,t,down}^{\mathrm{GU}}\end{pmatrix} \tag{36}$$

1) The constraint of power purchasing

The admissible boundaries of active and reactive power from the TN are as follows:

$$\begin{cases}0\le P_{e,t}^{\mathrm{TN}}\le P_{\max}^{\mathrm{TN}}\\ 0\le Q_{e,t}^{\mathrm{TN}}\le Q_{\max}^{\mathrm{TN}}\end{cases},\forall e\in\Omega^{\mathrm{TN}},\forall t \tag{37}$$

2) The re-dispatch constraints of the GUs

Notably, the GUs located in the typhoon area are not attacked due to the solid infrastructure construction and the advanced communication technology of the DN. Limited by the allowable upward/downward ramp rate, the generation curtailment of the GUs is considered as shown in Fig. 4. Hence, the re-dispatch constraints of GUs are as follows:

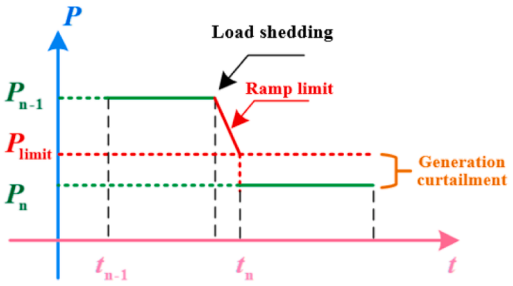

Fig. 4. The re-dispatch of GUs in the response stage.

$$\delta_{g,t}P_{g,\min}^{\mathrm{GU}}\le P_{g,t}^{\mathrm{GU}}+P_{g,t,\mathrm{up}}^{\mathrm{GU}}-P_{g,t,\mathrm{down}}^{\mathrm{GU}}\le\delta_{g,t}P_{g,\max}^{\mathrm{GU}},\forall g\in\Omega^{\mathrm{GU}},\forall t \tag{38}$$

$$\left(P_{g,t}^{\mathrm{GU}}+P_{g,t,\mathrm{up}}^{\mathrm{GU}}-P_{g,t,\mathrm{down}}^{\mathrm{GU}}\right)-\left(P_{g,t-1}^{\mathrm{GU}}+P_{g,t-1,\mathrm{up}}^{\mathrm{GU}}-P_{g,t-1,\mathrm{down}}^{\mathrm{GU}}\right)\le R_g^{\mathrm{up}},\forall g\in\Omega^{\mathrm{GU}},\forall t \tag{39}$$

$$\left(P_{g,t-1}^{\mathrm{GU}}+P_{g,t-1,\mathrm{up}}^{\mathrm{GU}}-P_{g,t-1,\mathrm{down}}^{\mathrm{GU}}\right)-\left(P_{g,t}^{\mathrm{GU}}+P_{g,t,\mathrm{up}}^{\mathrm{GU}}-P_{g,t,\mathrm{down}}^{\mathrm{GU}}\right)\le R_g^{\mathrm{down}},\forall g\in\Omega^{\mathrm{GU}},\forall t \tag{40}$$

$$0\le P_{g,t,\mathrm{up}}^{\mathrm{GU}}\le D_{g,t}^{\mathrm{up}},\forall g\in\Omega^{\mathrm{GU}},\forall t \tag{41}$$

$$0\le P_{g,t,\mathrm{down}}^{\mathrm{GU}}\le D_{g,t}^{\mathrm{down}},\forall g\in\Omega^{\mathrm{GU}},\forall t \tag{42}$$

$$0\le P_{g,t,\mathrm{cur}}^{\mathrm{GU}}\le P_{g,t}^{\mathrm{GU}},\forall g\in\Omega^{\mathrm{GU}},\forall t \tag{43}$$

$$Q_{g,t,\max}^{\mathrm{GU}}=\left(P_{g,t}^{\mathrm{GU}}+P_{g,t,\mathrm{up}}^{\mathrm{GU}}-P_{g,t,\mathrm{down}}^{\mathrm{GU}}-P_{g,t,\mathrm{cur}}^{\mathrm{GU}}\right)\tan\left(\cos^{-1}(\mathrm{pf}_1)\right),\forall g\in\Omega^{\mathrm{GU}},\forall t \tag{44}$$

$$-Q_{g,t,\max}^{\mathrm{GU}}\le Q_{g,t}^{\mathrm{GU}}+\Delta Q_{g,t}^{\mathrm{GU}}\le Q_{g,t,\max}^{\mathrm{GU}},\forall g\in\Omega^{\mathrm{GU}},\forall t \tag{45}$$

where the real-time output of the GU is limited by Constraint (38). Constraints (39) and (40) represent the upward and downward ramp limits of the GU. Constraints (41) and (42) denote that the power adjustment of the GU is limited by its reserve capacity. Constraint (43) denotes the limit of generation curtailment. The reactive power output of the GU is given by Constraints (44) and (45).

3) The operation constraints of the BSS

The BSS can not only restore the critical load by discharging power and reduce the generation curtailment of the GUs by charging power, but also provide reactive power compensation according to the rated capacity. The operation constraints of the BSS are as follows:

$$\left(P_{b,t,\mathrm{ch}}^{\mathrm{BSS}}\eta_{\mathrm{ch}}\right)^2+\left(Q_{b,t}^{\mathrm{BSS}}\right)^2\le\left(S_b^{\mathrm{BSS}}\right)^2,\forall b\in\Omega^{\mathrm{BSS}},\forall t \tag{46}$$

$$\left(P_{b,t,\mathrm{dis}}^{\mathrm{BSS}}\eta_{\mathrm{dis}}\right)^2+\left(Q_{b,t}^{\mathrm{BSS}}\right)^2\le\left(S_b^{\mathrm{BSS}}\right)^2,\forall b\in\Omega^{\mathrm{BSS}},\forall t \tag{47}$$

$$\beta_{b,t,\mathrm{ch}}^{\mathrm{BSS}}+\beta_{b,t,\mathrm{dis}}^{\mathrm{BSS}}\le 1,\forall b\in\Omega^{\mathrm{BSS}},\forall t \tag{48}$$

$$0\le P_{b,t,\mathrm{ch}}^{\mathrm{BSS}}\eta_{\mathrm{ch}}\le\beta_{b,t,\mathrm{ch}}^{\mathrm{BSS}}S_b^{\mathrm{BSS}},\forall b\in\Omega^{\mathrm{BSS}},\forall t \tag{49}$$

$$0\le P_{b,t,\mathrm{dis}}^{\mathrm{BSS}}\eta_{\mathrm{dis}}\le\beta_{b,t,\mathrm{dis}}^{\mathrm{BSS}}S_b^{\mathrm{BSS}},\forall b\in\Omega^{\mathrm{BSS}},\forall t \tag{50}$$

$$E_{b,t+1}^{\mathrm{BSS}} = E_{b,t}^{\mathrm{BSS}} + P_{b,t,\mathrm{ch}}^{\mathrm{BSS}}\eta_{\mathrm{ch}} - P_{b,t,\mathrm{dis}}^{\mathrm{BSS}}\eta_{\mathrm{dis}}, \forall b \in \Omega^{\mathrm{BSS}}, \forall t \tag{51}$$

$$\left(1-\sigma^{\mathrm{BSS}}\right)E_{b}^{\mathrm{BSS}} \le E_{b,t}^{\mathrm{BSS}} \le E_{b}^{\mathrm{BSS}}, \forall b \in \Omega^{\mathrm{BSS}}, \forall t \tag{52}$$

$$E_{b,1}^{\mathrm{BSS}} = \nu^{\mathrm{BSS}}E_{b}^{\mathrm{BSS}}, \forall b \in \Omega^{\mathrm{BSS}} \tag{53}$$

where Eqs. (46) and (47) limit the active and reactive power of the BSS. Eqs. (48)-(50) prevent the BSS from charging and discharging power at the same time. The energy level of the BSS is expressed in Eq. (51). Constraint (52) sets the minimum and the maximum limits of the energy storage. Expression (53) gives the initial energy level.

4) The operation constraints of the SOP

As a fully controllable power electronic device, the SOP has different kinds of work modes, which can adjust the power flow of the DN quickly and continuously [11]. Compared with the exchanged power among feeders connected by the SOP, the power losses of source converters are so small that they can be ignored. Therefore, the operation constraints of the SOP are as follows:

$$P_{s,t}^{\mathrm{SOP}} + P_{q,t}^{\mathrm{SOP}} = 0, \forall s,q \in \Omega^{\mathrm{SOP}}, \forall t \tag{54}$$

$$\sqrt{\left(P_{s,t}^{\mathrm{SOP}}\right)^2 + \left(Q_{s,t}^{\mathrm{SOP}}\right)^2} \le S_{s}^{\mathrm{SOP}}, \forall s \in \Omega^{\mathrm{SOP}}, \forall t \tag{55}$$

$$\sqrt{\left(P_{q,t}^{\mathrm{SOP}}\right)^2 + \left(Q_{q,t}^{\mathrm{SOP}}\right)^2} \le S_{q}^{\mathrm{SOP}}, \forall q \in \Omega^{\mathrm{SOP}}, \forall t \tag{56}$$

$$U_{s,t}^{SOP} \ge U_0, \forall s \in \Omega^{SOP}, \forall t \tag{57}$$

where Eq. (54) ensures the power flow balance of the SOP without considering its power losses. Constraints (55) and (56) limit the active and reactive power outputs of the SOP. Constraint (57) requires the voltage on the side of the SOP connected with the critical load.

5) The constraints of load shedding

$$0 \le P_{i,t,\mathrm{sh}}^{\mathrm{Load}} \le P_{i,t}^{\mathrm{Load}}, \forall i \in \Omega^{\mathrm{DN}}, \forall t \tag{58}$$

$$Q_{i,t,\mathrm{sh}}^{\mathrm{Load}} = \left(P_{i,t,\mathrm{sh}}^{\mathrm{Load}} \Big/ P_{i,t}^{\mathrm{Load}}\right)Q_{i,t}^{\mathrm{Load}}, \forall i \in \Omega^{\mathrm{DN}}, \forall t \tag{59}$$

6) The constraints of linear power flow

The power flow constraints for the resilient DN can be represented by the linearized DistFlow model used in [34], which is represented as follows:

$$\begin{aligned} P_{i,t} = &\sum_{h\in\Omega^{\mathrm{TN}}} P_{h,t}^{\mathrm{TN}} + \sum_{b\in\Omega^{\mathrm{BSS}}}\left(P_{b,t,\mathrm{ch}}^{\mathrm{BSS}} - P_{b,t,\mathrm{dis}}^{\mathrm{BSS}}\right) + \sum_{s\in\Omega^{\mathrm{SOP}}} P_{s,t}^{\mathrm{SOP}} \\ &+ \sum_{g\in\Omega^{\mathrm{GU}}}\left(P_{g,t}^{\mathrm{GU}} + P_{g,t,\mathrm{up}}^{\mathrm{GU}} - P_{g,t,\mathrm{down}}^{\mathrm{GU}}\right) - \left(P_{i,t}^{\mathrm{Load}} - P_{i,t,\mathrm{sh}}^{\mathrm{Load}}\right), \forall i \in \Omega^{\mathrm{DN}}, \forall t \end{aligned} \tag{60}$$

$$\begin{aligned} Q_{i,t} = &\sum_{h\in\Omega^{\mathrm{TN}}} Q_{h,t}^{\mathrm{TN}} + \sum_{b\in\Omega^{\mathrm{BSS}}} Q_{b,t}^{\mathrm{BSS}} + \sum_{s\in\Omega^{\mathrm{SOP}}} Q_{s,t}^{\mathrm{SOP}} \\ &+ \sum_{g\in\Omega^{\mathrm{GU}}}\left(Q_{g,t}^{\mathrm{GU}} + \Delta Q_{g,t}^{\mathrm{GU}}\right) - \left(P_{i,t}^{\mathrm{Load}} - P_{i,t,\mathrm{sh}}^{\mathrm{Load}}\right), \forall i \in \Omega^{\mathrm{DN}}, \forall t \end{aligned} \tag{61}$$

$$\sum_{k\in\delta(j)} P_{jk,t} - \sum_{i\in\pi(j)} P_{ij,t} = P_{j,t}, \forall j \in \Omega^{\mathrm{DN}}, \forall t \tag{62}$$

$$\sum_{k\in\delta(j)} Q_{jk,t} - \sum_{i\in\pi(j)} Q_{ij,t} = Q_{j,t}, \forall j \in \Omega^{\mathrm{DN}}, \forall t \tag{63}$$

$$-P_{ij,\max}\theta_{ij,t} \le P_{ij,t} \le P_{ij,\max}\theta_{ij,t}, \forall ij \in \Omega^{\mathrm{BR}}, \forall t \tag{64}$$

$$-Q_{ij,\max}\theta_{ij,t} \le Q_{ij,t} \le Q_{ij,\max}\theta_{ij,t}, \forall ij \in \Omega^{\mathrm{BR}}, \forall t \tag{65}$$

$$U_{i,\min} \le U_{i,t} \le U_{i,\max}, \forall i \in \Omega^{\mathrm{DN}}, \forall t \tag{66}$$

$$U_{i,t} - U_{j,t} - \left(r_{ij}P_{ij,t} + x_{ij}Q_{ij,t}\right) / U_0 \le M\left(1-\theta_{ij,t}\right), \forall ij \in \Omega^{\mathrm{BR}}, \forall i \in \Omega^{\mathrm{DN}}, \forall t \tag{67}$$

$$U_{i,t} - U_{j,t} - \left(r_{ij}P_{ij,t} + x_{ij}Q_{ij,t}\right) / U_0 \ge -M\left(1-\theta_{ij,t}\right), \forall ij \in \Omega^{\mathrm{BR}}, \forall i \in \Omega^{\mathrm{DN}}, \forall t \tag{68}$$

where Constraints (60), (61) indicate the injection power of each bus. Constraints (62), (63) provide the power balance for the DN. Constraints (64)-(66) specify the limits of the line power capacity and bus voltage magnitude to ensure the safe operation of the DN. Constraints (67), (68) denote the relationship between the voltage drop of adjacent buses.

5. Solution methodology

The framework of the DN resilience enhancement is illustrated in Fig. 5, containing the typhoon events modeling and a resilience-oriented two-stage RO model. The former aims at constructing the multi-stage and multi-zone uncertainty set of vulnerable lines, which is as the input information for the RO model. The latter incorporates the planning-operational restoration and the RCUC into the prevention and emergency responses against typhoon attacks. Consequently, the two-stage RO model can be formulated as a mixed-integer linear programming problem by utilizing a polyhedral approximation method, which can be solved by the NC&CG algorithm.

5.1. Linearization method for the SOC constraints

Formulae (46), (47), (55), and (56) are the second-order cone (SOC) constraints, which make the proposed optimization problem non-convex. In order to obtain a tractable formulation, we approximate these constraints with 2N-sided polyhedral as shown in Fig. 6. The more sides we consider, the higher the approximation accuracy is. For clarity, a tight approximation preference is provided in Fig. 7 to select an appropriate number of sides in the engineering application. The adjustable polyhedral approximation can be expressed as follows:

$$\begin{cases} -S_b^{\mathrm{BSS}} \le \begin{bmatrix} P_{b,t,\mathrm{ch}}^{\mathrm{BSS}}, & Q_{b,t}^{\mathrm{BSS}} \end{bmatrix} \begin{bmatrix} \cos\varphi_b \\ \sin\varphi_b \end{bmatrix} \le S_b^{\mathrm{BSS}} \\ \varphi_b = n\dfrac{\pi}{N}, n = 1, \cdots, N \end{cases}, \forall b \in \Omega^{\mathrm{BSS}}, \forall t \tag{69}$$

$$\begin{cases} -S_b^{\mathrm{BSS}} \le \begin{bmatrix} P_{b,t,\mathrm{dis}}^{\mathrm{BSS}}, & Q_{b,t}^{\mathrm{BSS}} \end{bmatrix} \begin{bmatrix} \cos\varphi_b \\ \sin\varphi_b \end{bmatrix} \le S_b^{\mathrm{BSS}} \\ \varphi_b = n\dfrac{\pi}{N}, n = 1, \cdots, N \end{cases}, \forall b \in \Omega^{\mathrm{BSS}}, \forall t \tag{70}$$

$$\begin{cases} -S_s \le \begin{bmatrix} P_{s,t}, & Q_{s,t} \end{bmatrix} \begin{bmatrix} \cos\varphi_s \\ \sin\varphi_s \end{bmatrix} \le S_s \\ \varphi_s = n\dfrac{\pi}{N}, n = 1, \cdots, N \end{cases}, \forall s \in \Omega^{\mathrm{SOP}}, \forall t \tag{71}$$

$$\begin{cases} -S_q \le \begin{bmatrix} P_{q,t}, & Q_{q,t} \end{bmatrix} \begin{bmatrix} \cos\varphi_q \\ \sin\varphi_q \end{bmatrix} \le S_q \\ \varphi_q = n\dfrac{\pi}{N}, n = 1, \cdots, N \end{cases}, \forall q \in \Omega^{\mathrm{SOP}}, \forall t \tag{72}$$

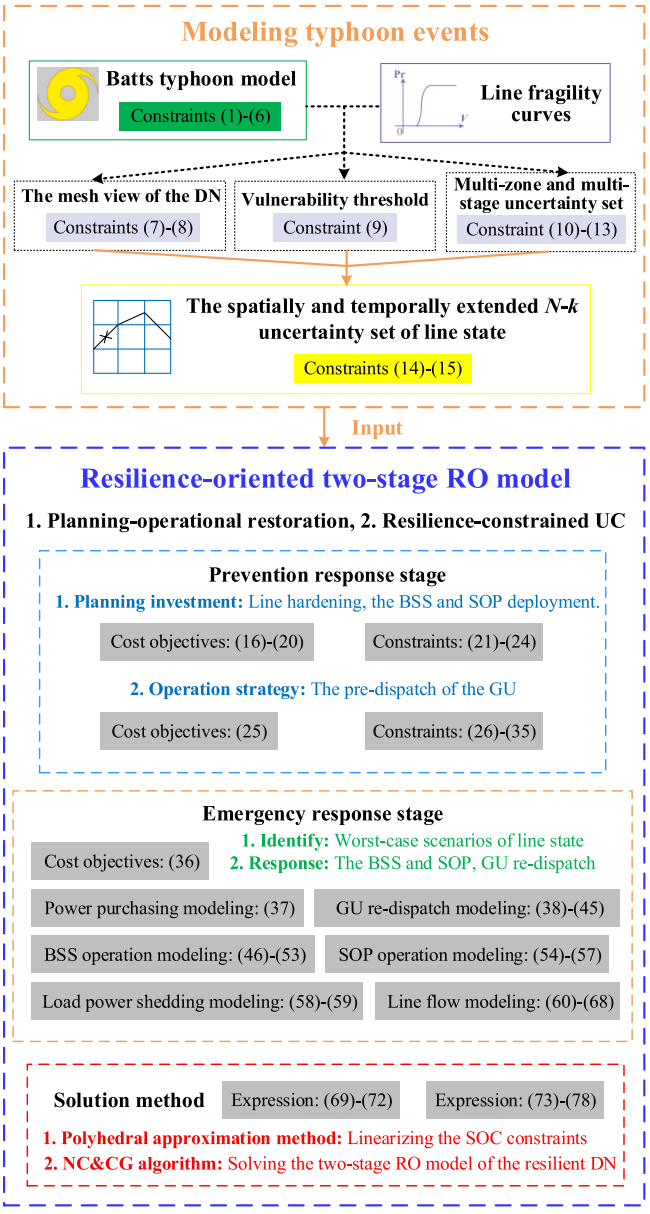

Fig. 5. The framework of the resilience enhancement.

5.2. Solution for the two-stage RO model

In the resilience-oriented two-stage RO model, the binary variables of the BSS are considered as the second-stage (wait-and-see) decisions, which is more consistent with the fact that a fast response is conducive to enhancing the DN resilience. For notational brevity, the proposed model (10)-(72) can be expressed with a compact matrix form as follows:

$$\min_{x_1,x_2\in X}\left({a_1}^{\mathrm{T}}x_1+{a_2}^{\mathrm{T}}x_2+\max_{u\in U_l}\min_{y_1,y_2\in Y(X,u)}b^{\mathrm{T}}y_2\right) \tag{73a}$$

$$s.t.\ \ A_1x_1+A_2x_2\le c \tag{73b}$$

$$B_1x_1+B_2x_2+C_1y_1+C_2y_2=d \tag{73c}$$

$$D_1x_1+D_2x_2+E_1y_1+E_2y_2+Fu\le e \tag{73d}$$

$$G_1y_1+G_2y_2\le g \tag{73e}$$

where x_1 and x_2 represent the planning and operation variables in the prevention response stage, respectively. The uncertain vector u represents the line status. y_1 and y_2 are the discrete and continuous decision vectors in the emergency response stage, respectively. $Y(X,u)$ is the feasible region of y_1 and y_2 for the given (x_1,x_2,u).

5.2.1. The master problem

The tri-level optimization problem (73) is a mixed-integer linear programming problem, which cannot be directly solved by the traditional column-and-constraint generation (C&CG) method due to the binary variables at the innermost level. Fortunately, an NC&CG algorithm can be used to address this difficulty. To obtain the tractable formulations, the original problem (73) is decomposed into a single-level "min" problem as the master problem (MP) and a bi-level "max-min" problem as the sub-problem (SP). Under the given worst-case scenario and the added event-related constraints, the MP can be expressed as follows:

$$\mathrm{MP}:\ \ \delta_{\mathrm{MP}}^{\mathrm{NC\&CG}}=\min_{x_1,x_2\in X}{a_1}^{\mathrm{T}}x_1+{a_2}^{\mathrm{T}}x_2+f \tag{74a}$$

$$s.t.\ \ A_1x_1+A_2x_2\le c \tag{74b}$$

$$b^{\mathrm{T}}y_2^{l_1}\le f,\forall l_1\le n \tag{74c}$$

$$B_1x_1+B_2x_2+C_1y_1^{l_1}+C_2y_2^{l_1}=d,\forall l_1\le n \tag{74d}$$

$$D_1x_1+D_2x_2+E_1y_1^{l_1}+E_2y_2^{l_1}+Fu^{*l_1}\le e,\forall l_1\le n \tag{74e}$$

$$G_1y_1^{l_1}+G_2y_2^{l_1}\le g,\forall l_1\le n \tag{74f}$$

where l_1 and n are the index of the constraints and the iteration number of the MP respectively. f is an introduced scalar variable. The MP will be iteratively solved to provide the lower bound for the original problem (73).

5.2.2. The sub-problem problem

Based on the optimal solution x_1^* and x_2^* derived from the MP, the SP can be expressed as follows:

$$SP:\delta_{\mathrm{SP}}^{\mathrm{NC\&CG}}=\max_{u\in U_l}\min_{y_1,y_2\in Y(X,u)}b^{\mathrm{T}}y_2 \tag{75a}$$

$$s.t.\ \ B_1x_1^*+B_2x_2^*+C_1y_1+C_2y_2=d \tag{75b}$$

$$D_1x_1^*+D_2x_2^*+E_1y_1+E_2y_2+Fu\le e \tag{75c}$$

$$G_1y_1+G_2y_2\le g \tag{75d}$$

Since the inner "min" problem in (75) is a mixed integer programming problem, the bi-level "max-min" problem cannot be reformulated as a single-level "max" problem by strong duality theory [13]. To address this difficulty, the SP (75) is rewritten as a tri-level problem (76) by separating binary variables from continuous variables.

$$\max_{u\in U_l}\min_{y_1\in Y(X,u)}\min_{y_2\in Y(X,u)}b^{\mathrm{T}}y_2 \tag{76a}$$

$$s.t.\ \text{(75b)-(75d) (76b)}$$

At this time, the strong duality theory holds for the continuous variables. The tri-level problem (76) is decomposed into the inner-sub-problem (77) and the inner-master problem (78), respectively.

1) The inner-sub-problem (ISP)

$$\delta_{\mathrm{ISP}}^{\mathrm{NC\&CG}}=\min_{y_1,y_2}b^{\mathrm{T}}y_2 \tag{77a}$$

$$s.t.\ \ C_2y_2=d-B_1x_1^*-B_2x_2^*-C_1y_1:\ \ \pi_1 \tag{77b}$$

$$E_2y_2\le e-D_1x_1^*-D_2x_2^*-E_1y_1-Fu^*:\ \ \pi_2 \tag{77c}$$

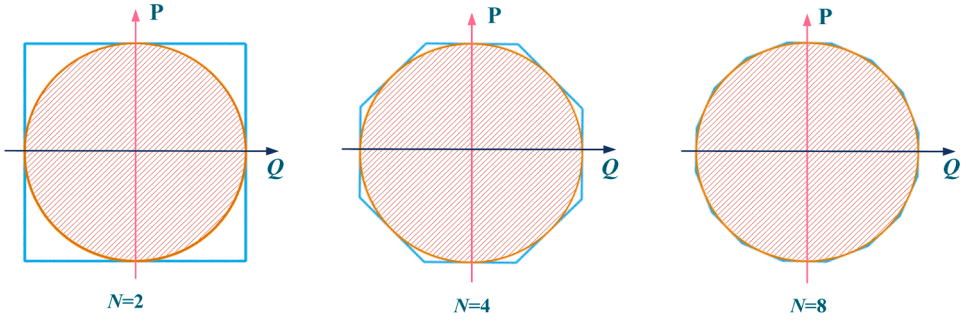

Fig. 6. Polyhedral approximation of SOC constraints.

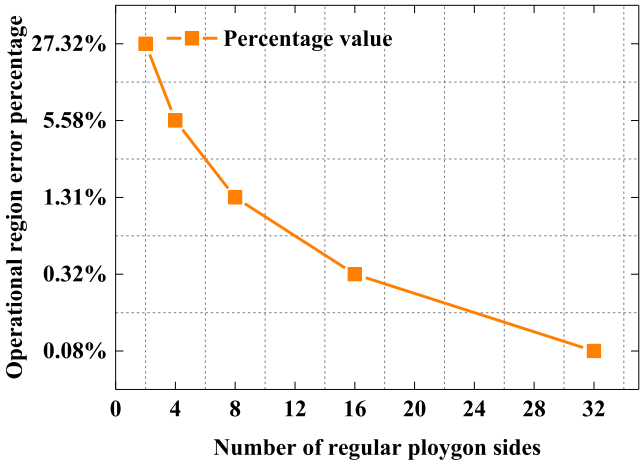

Fig. 7. Error percentage of different sided polyhedral approximations.

$$G_2 y_2 \le g - G_1 y_1 : \quad \pi_2 \tag{77d}$$

where π_1, π_2, and π_3 are the dual vectors for Constraints (77b), (77c), and (77d), respectively.

2) The inner-master problem (IMP)

$$\delta_{\mathrm{IMP}}^{\mathrm{NC\&CG}} = \max_{\pi_1,\pi_2,\pi_3} \theta \tag{78a}$$

$$s.t. \quad \theta \le \begin{pmatrix} \left(d - B_1 x_1^* - B_2 x_2^* - C_1 y_1^{*l_2}\right)^{\mathrm{T}} \pi_1^{l_2} - \\ \left(e - D_1 x_1^* - D_2 x_2^* - E_1 y_1^{*l_2} - Fu\right)^{\mathrm{T}} \pi_2^{l_2} \\ + \left(g - G_1 y_1^{*l_2}\right)^{\mathrm{T}} \pi_3^{l_2} \end{pmatrix}, \forall l_2 \le m \tag{78b}$$

$$C_2^{\mathrm{T}} \pi_1^{l_2} + E_2^{\mathrm{T}} \pi_2^{l_2} + G_2^{\mathrm{T}} \pi_3^{l_2} \le b, \forall l_2 \le m \tag{78c}$$

$$\pi_2^{l_2}, \pi_3^{l_2} \le 0, \forall l_2 \le m \tag{78d}$$

$$\pi_1^{l_2} : \text{free}, \forall l_2 \le m \tag{78e}$$

where l_2 and m are the index of the constraints and the iteration number of the iteration, respectively. The bilinear terms $u^{\mathrm{T}} F^{\mathrm{T}} \pi_2^{l_2}$ in (78b) can be linearized by the big-M method [35].

The NC&CG algorithm is employed to solve the tri-level mixed-integer linear programming problem. The detailed solution procedure consists of two nested loop frameworks as shown in Fig. 8, where the sub-problem can be solved in the inner loop to provide the upper bound and its optimal solution is generated in an interactive iteration manner. In addition, after iteratively adding the corresponding constraints to the master problem in the outer loop, the master problem can be incessantly updated until the optimal solution to the original problem is found.

6. Case study

6.1. Simulation parameters

In this section, the modified IEEE 33-bus DN is utilized to verify the effectiveness of the proposed model and method [36]. It is assumed that the system is located in the coastal areas of Fujian province, China, approximately within the geographical position (117.55°E-119.04°E, 24.38°N-25.94°N). Based on the statistical records of typhoon path [37], the power system is divided into three geographical zones as illustrated in Fig. 9. Based on the bi-normal distribution of the landing direction angle and the logarithmic normal distribution of the landing motion speed [32], the Monte Carlo method is adopted to generate the invasion angle and moving speed for the Batts typhoon model. The vulnerability threshold of each overhead line is set as 4%. The resilience-oriented optimal scheduling of the DN is conducted within 1 h and the time interval is 5 min.

The system-rated voltage level is 12.66kV, and the voltage range of each bus is set as [0.90, 1.10]. The critical power users are located at buses 10, 19, 24, 26, 29, and 32, respectively, and the non-critical power users are at other buses. The penalty cost of non-critical load shedding is set to $5000/MW while the penalty cost of critical load shedding is 100 times as much as it. The cost of the line hardening is 240,000$/km. The electricity price of the TN is 420$/MW. The budget for the number of hardening lines is 4. The lifetime of the BSS, SOP, and hardened lines are 20, 20, and 50 years, respectively. The yearly interest rate is 0.1. In addition, the other parameters of the BSS and SOP are listed in Table 1. The parameters of the GUs are presented in Table 2. The load profiles are shown in Fig. 10.

The proposed model is carried out on the MATLAB/YALMIP simulation platform and is solved by the CPLEX solver. The optimality gap for CPLEX is set as 0.02%. All simulation tests are executed on a laptop computer with Intel (R) Core (TM) i9-10855H CPU @ 2.40 GHz 16.00GB RAM.

6.2. Evaluation of the typhoon attacks

To evaluate the impact of typhoons on the DN, we use the Monte Carlo method to simulate 500 typhoon attack events, where the top 6 events are shown in Table 3. Then, we solve the resilience-oriented two-stage RO model with the scenarios of the top 6 typhoon events, respectively. The simulation results are listed in Tables 4-6. As illustrated in Table 4, there are some worst-case contingencies in common in the case of the top 6 events, such as the outage of lines 16-17, 17-18, and

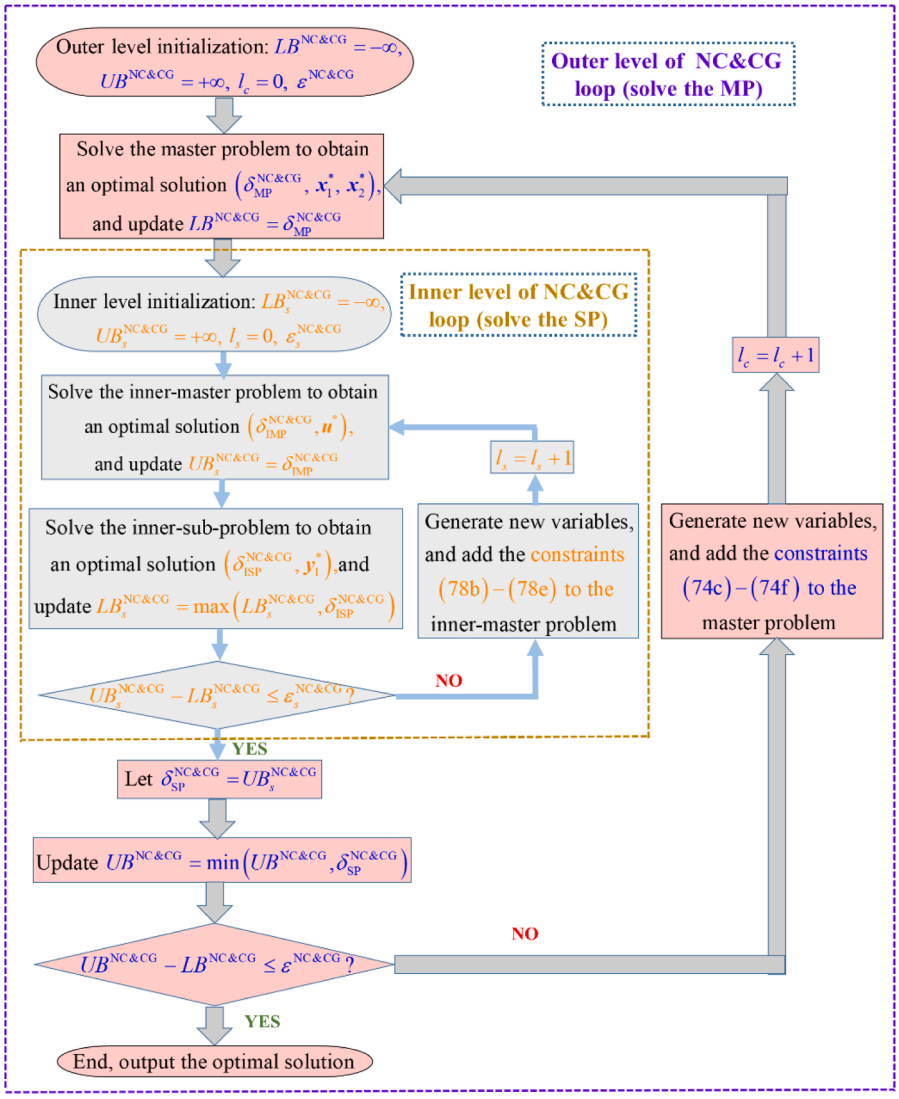

Fig. 8. Flow chart of the NC&CG method.

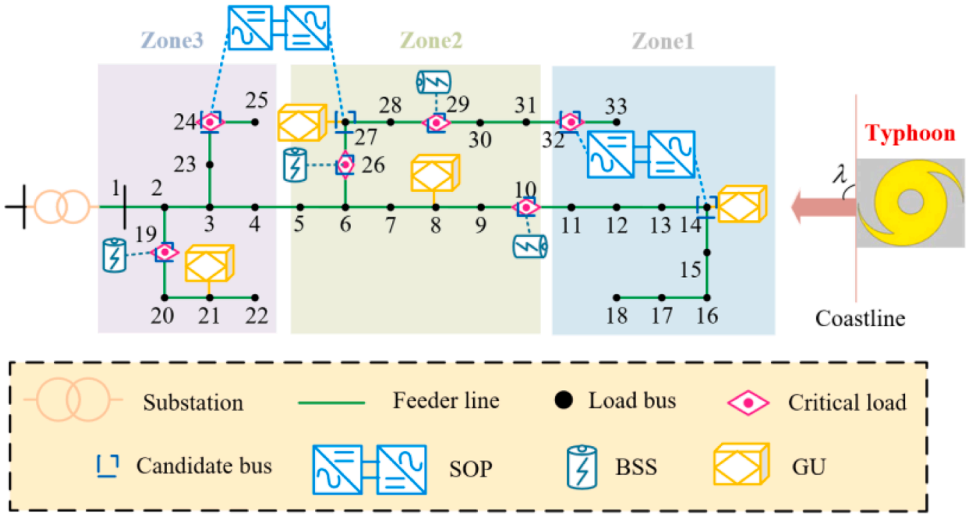

Fig. 9. Schematic of the DN.

Table 1
The parameters of BSS and SOP.

Parameter	Values	Parameter	Values
k_S	100,000$/MVA	ν^{BSS}	0.3
k_E	200,000$/MW	$E^{BSS}_{i,max}$	1MWh
k_M	0.01	r_S	150,000$/MVA
σ^{BSS}	0.2	r_M	0.01
$S^{BSS}_{i,max}$	0.5MVA	$S^{SOP}_{i,max}$	1MVA

Table 2
The parameters of the GUs.

Parameter	GU1	GU2	GU3	GU4
$\chi_{i,1}$	1	0	0	1
$T^{on}_{i,min}$ /$T^{off}_{i,min}$(min)	15/10	10/5	15/10	15/10
R^{up}_i /R^{down}_i(MW)	0.42	0.48	0.66	0.42
$P^{GU}_{i,min}$ /$P^{GU}_{i,max}$(MW)	0.15/0.70	0.30/0.80	0.15/0.90	0.30/0.90
c^{GU}_i($/MW)	60	65	55	60
c^{on}_i /c^{off}_i($/MW)	20	25	15	20
c^{up}_i /c^{down}_i($/MW)	30	25	25	30
c^{GU}_{cur}($/MW)	4000	3500	4000	4500
$c^{GU}_{i,up}$ /$c^{GU}_{i,down}$($/MW)	160	170	180	170

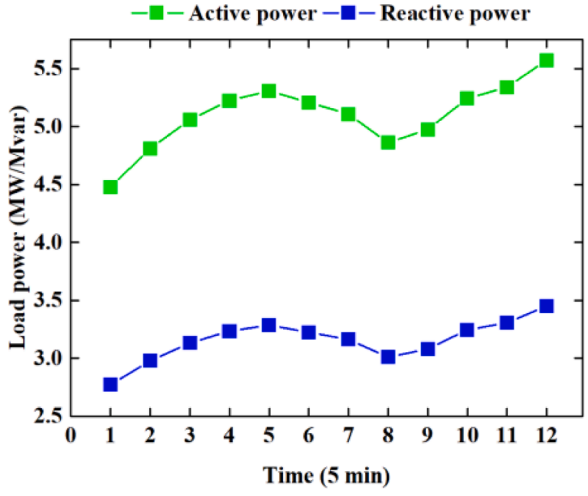

Fig. 10. The forecast profile of load power.

Table 3
The top 6 of the typhoon attack events.

Rank	Frequency	Number of vulnerable lines		
		Zone1	Zone2	Zone3
#1	10.21%	4	4	4
#2	9.53%	4	3	3
#3	8.12%	3	2	2
#4	7.65%	5	4	3
#5	7.26%	4	3	2
#6	6.76%	3	3	2

Table 4
The worst-case scenarios of the damaged lines.

Rank	Damaged lines		
	Zone1	Zone2	Zone3
#1	15-16, 16-17, 17-18, 32-33	26-27, 29-30, 30-31, 31-32	21-22, 3-23, 23-24, 24-25
#2	15-16, 16-17, 17-18, 32-33	29-30, 30-31, 31-32	3-23, 23-24, 24-25
#3	16-17, 17-18, 32-33	30-31, 31-32	23-24, 24-25
#4	14-15, 15-16, 16-17, 17-18, 32-33	26-27, 29-30, 30-31, 31-32	3-23, 23-24, 24-25
#5	15-16, 16-17, 17-18, 32-33	29-30, 30-31, 31-32	23-24, 24-25
#6	16-17, 17-18, 32-33	29-30, 30-31, 31-32	23-24, 24-25

Table 5
The optimal results for the RO model related to the top 6 events.

Rank	Hardened lines	Non-critical load shedding (MW)	Total investment costs ($)
#1	27-28, 28-29	11.95	200,717.61
#2	None	11.27	38,051.93
#3	None	7.53	38,051.93
#4	27-28, 28-29	12.43	200,717.61
#5	None	10.76	38,051.93
#6	None	7.53	38,051.93

32-33 in Zone 1, which can help us evaluate the weak components of the DN. As shown in Table 5, the investment costs and hardened lines for Rank #1 and #4 are the same while those for Rank #2, #3, #5, and #6 are consistent, which means that a prevention strategy can respond with different worst-case outages. In addition, the total costs and calculation time for the RO model related to the top 6 events are listed in Table 6.

6.3. Comparison of different cases

To demonstrate the advantage of the proposed comprehensive planning-operation strategy, the following two cases are investigated.

Case 1: In the resilience-oriented two-stage RO model, we only consider the resilience-constrained unit commitment for the DN resilience enhancement [13,14].

Case 2: In the resilience-oriented two-stage RO model, we develop a comprehensive planning-operation strategy as mentioned in Section 4 for the DN resilience enhancement.

In the above cases, we assume that the budget for the number of hardened lines is 2 and the number of vulnerable lines in each zone is 7. The models in Case 1 and Case 2 are solved by the C&CG [25] and NC&CG methods, respectively. As a result, the overhead line status during the typhoon is shown in Fig. 11. To improve the DN resilience, Lines 3-23 and 23-24 are hardened in Case 1 while Lines 27-28 and 28-29 are hardened in Case 2. Compared to Case 1, the hardened lines located in Zone 2 in Case 2 are attacked by the typhoon earlier than Zone 1, which can reduce the amount of load shedding. In addition, the dispatch schemes of the GU in Cases 1 and 2 are shown in Figs. 12 and 13, respectively. Compared to Case 1, Case 2 can reduce the generation curtailment of the GU by the less reserve capacity.

As shown in Tables 7 and 8, the load shedding and generation curtailment have been mitigated by deploying the BSS and SOP in Case 2 compared to Case 1. As a result, Case 2 has better economic performance than Case 1, which can be seen in Table 9. Meanwhile, more

Table 6
Total costs and calculation time for the RO model related to the top 6 events.

Rank	#1	#2	#3	#4	#5	#6
Total costs ($)	531754.09	353448.63	267798.55	542660.21	341726.70	267798.55
Calculation time (s)	277.00	196.43	198.45	289.78	185.47	181.95

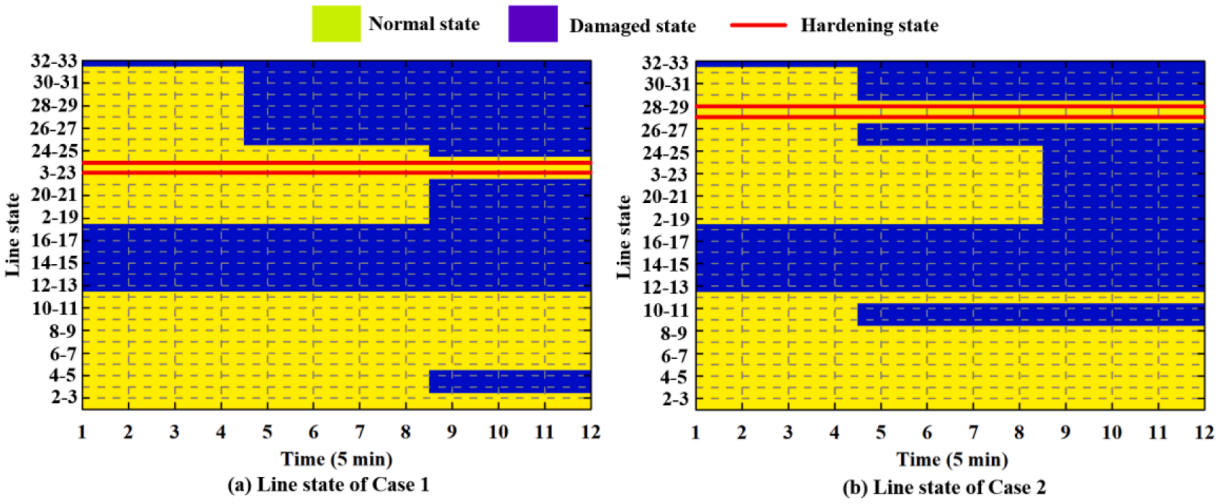

Fig. 11. Line status of Case 1 and Case 2.

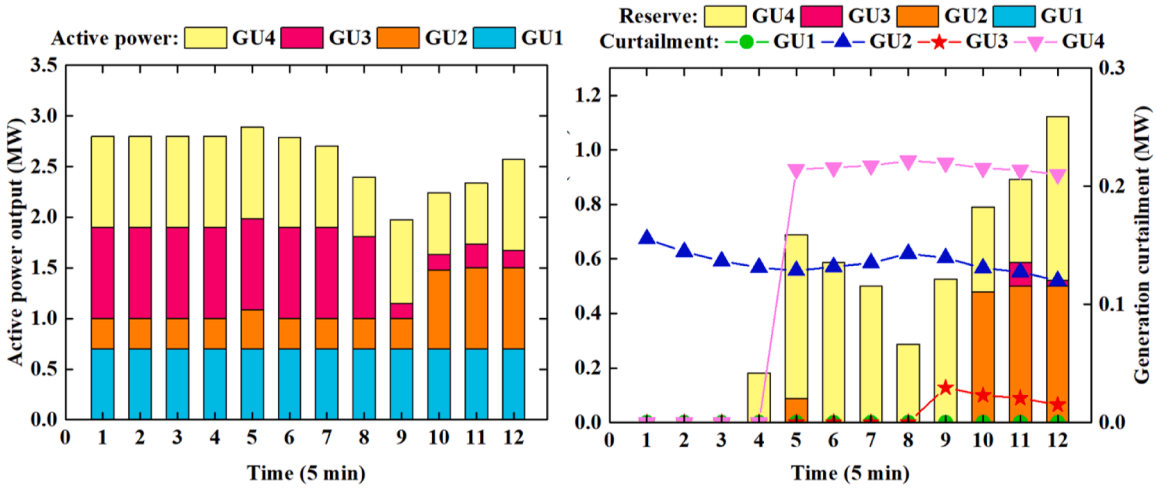

Fig. 12. The dispatch strategy of the GU in Case 1.

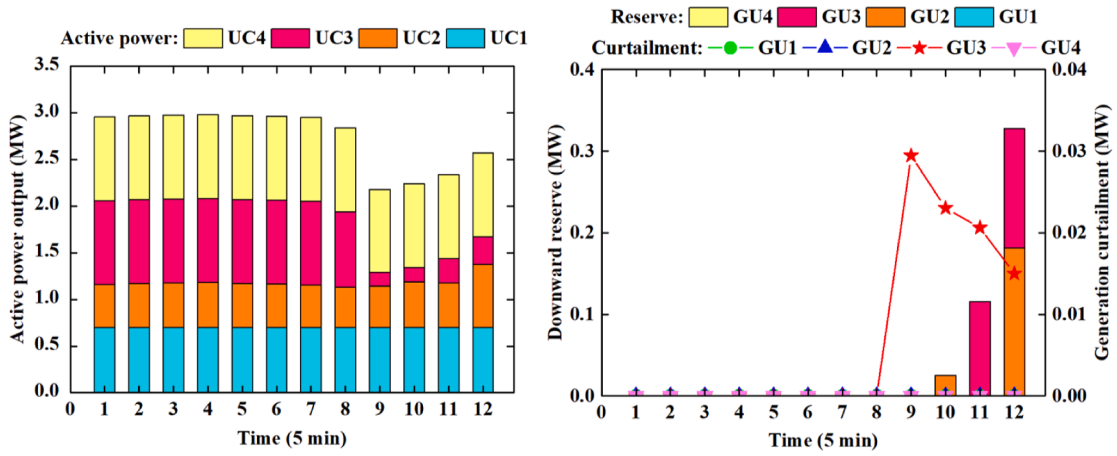

Fig. 13. The dispatch strategy of the GU in Case 2.

Table 7
Penalty costs of Case 1 and Case 2.

	Critical load shedding ($)	Non-critical load shedding ($)	Generation curtailment ($)
Case 1	12,200,558.05	413,684.15	69,056.90
Case 2	210,267.86	390,335.38	1762.50

Table 8
Planning-operation costs of Case 1 and Case 2.

	Hardened line ($)	SOP and BSS deployment ($)	GU operation ($)	Power purchasing from the TN ($)
Case 1	151,046.70	/	15,003.42	37,093.64
Case 2	162,665.68	110,643.08	10,500.97	28,361.06

Table 9
Total cost and calculation time of Case 1 and Case 2.

	Total cost ($)	Calculation time (s)
Case 1	12,886,443.22	90.30
Case 2	914,536.54	174.57

observations about the operation strategies for the BSS and SOP are illustrated in Figs. 14 and 15.

6.4. Sensitivity analysis

To explore the impacts of line hardening budgets and typhoon attacks on the resilient DN, a sensitivity analysis for the resilience-oriented RO model in Case 2 is further performed. The configuration capacity of the BSS and SOP is presented in Table 10. With the higher typhoon attack level, the larger capacity of the BSS is configured to provide the power supply for load demand in islands while the capacity of the SOP does not change. More specifically, the optimal planning strategies against the identified worst-case scenarios of the outages are given in Fig. 16. No lines are hardened when $N_{l,max} = 1$ and k_ω is set to 5 and 6. The reason is that when economic benefit brought by the load recovery is less than the investment cost of line hardening, a more cost-effective decision without line hardening is obtained.

In addition, the numerical results listed in Table 11 indicate a monotonically decreasing trend of load shedding with the increase of hardening budgets or the decline of typhoon attack levels, while the generation curtailment of the GU remains unchanged. Furthermore, the computation time and optimal results for the RO model are shown in Table 12. As the hardening budget raises, the total cost is reduced but computational efficiency may be sacrificed. Such results of the sensitivity analysis can guide decision-makers to determine a proper planning-operation strategy for the resilient DN in response to typhoon attacks.

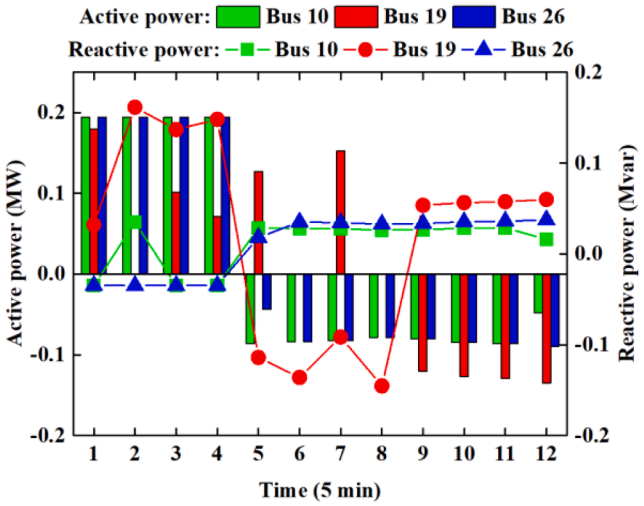

Fig. 14. The operation strategy of the BSS in Case 2.

7. Conclusions

To improve the DN resilience, this paper proposes a resilience-oriented two-stage RO model in a minute-level scheduling framework, which is solved by the NC&CG method. Numerical studies in Section 6 illustrate the effectiveness of the proposed model and approach. The conclusions are summarized as follows:

1) The simulation results indicate that the proposed spatially and temporally extended N-k uncertainty set can capture the typhoon impact on the DN over time and space. Besides, through the simulation and evaluation of the sequential typhoon attacks, the weak parts of the DN can be identified in advance of the typhoon, which can provide a guidance to make an effective resilience-oriented defense strategy for the upcoming typhoon.

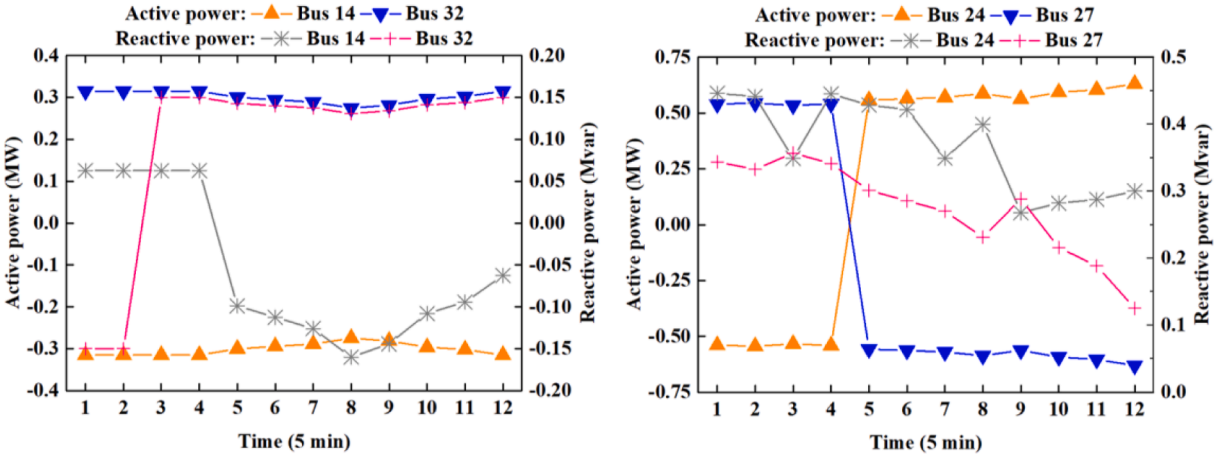

Fig. 15. The operation strategy of the SOP in Case 2.

Table 10
SOP and BSS capacities under various hardening budgets and typhoon attack levels.

k_{ϖ}	7			6			5		
$N_{l,\max}$	1	2	3	1	2	3	1	2	3
S_i^{BSS}	0.000	0.175	0.175	0.000	0.000	0.000	0.000	0.000	0.000
(MVA)	0.162	0.162	0.162	0.000	0.000	0.000	0.000	0.000	0.000
	0.000	0.175	0.000	0.000	0.175	0.175	0.000	0.175	0.000
	0.175	0.000	0.000	0.175	0.000	0.000	0.175	0.000	0.000
E_i^{BSS}	0.000	1.000	1.000	0.000	0.000	0.000	0.000	0.000	0.000
(MWh)	0.813	0.813	0.813	0.000	0.000	0.000	0.000	0.000	0.000
	0.000	1.000	0.000	0.000	1.000	1.000	0.000	1.000	0.000
	1.000	0.000	0.000	1.000	0.000	0.000	1.000	0.000	0.000
S_i^{SOP}	0.315	0.315	0.315	0.315	0.315	0.315	0.315	0.315	0.315
(MVA)	0.348	0.348	0.348	0.348	0.348	0.348	0.348	0.348	0.348
	0.697	0.697	0.697	0.697	0.697	0.697	0.697	0.697	0.697
	0.630	0.630	0.630	0.630	0.630	0.630	0.630	0.630	0.630

Declare: The BSSs are installed on buses 10, 19, 26, and 29, respectively. The SOPs are installed on buses 14, 32, 24, and 27, respectively. The GUs are installed on buses 8, 14, 21, and 27, respectively.

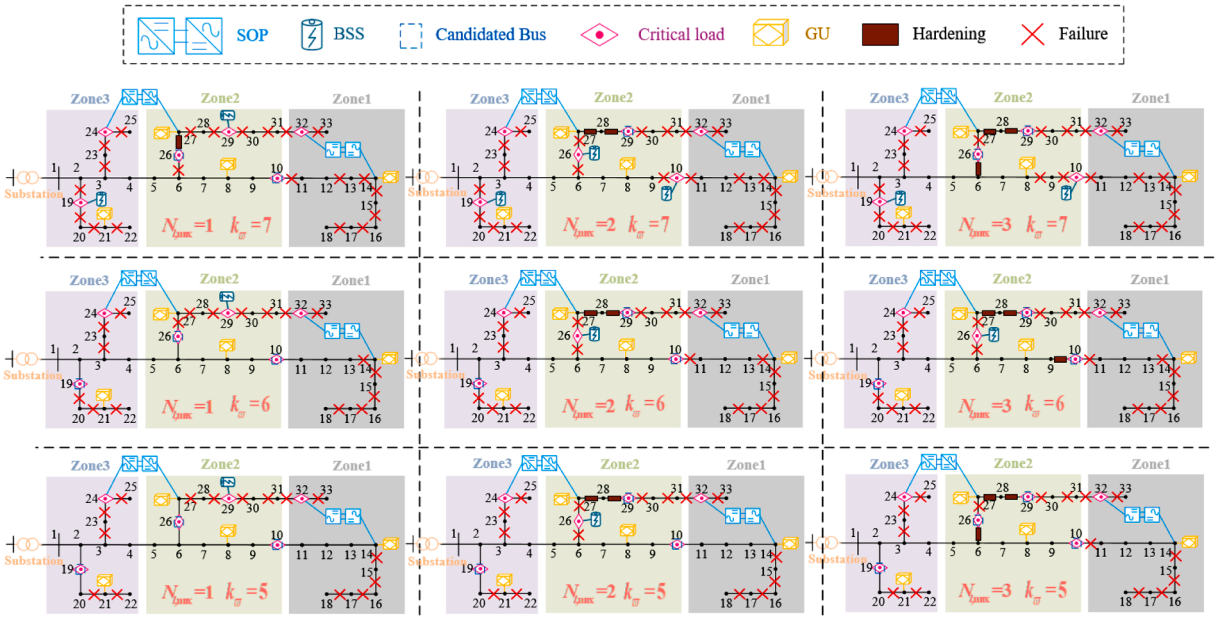

Fig. 16. Planning strategies against the identified worst-case scenarios of the typhoon attacks.

Table 11
Load shedding and generation curtailment under various hardening budgets and typhoon attack levels.

k_{ϖ}	$N_{l,\max}$	Resilience-oriented two-stage RO model (Case 2)		
		Critical load shedding (MW)	Noncritical load shedding (MW)	Generation curtailment (MW)
7	1	0.7141	16.116	0.0881
	2	0.0841	15.613	0.0881
	3	0.0421	16.2855	0.0881
6	1	0.7141	13.9514	0.0881
	2	0.0421	15.2973	0.0881
	3	0.0421	15.2973	0.0881
5	1	0.7141	13.4396	0.0881
	2	0.0421	12.9373	0.0881
	3	0	12.9373	0.0881

Table 12
Computation time and optimal result for the RO model.

k_{ϖ}	$N_{l,\max}$	Resilience-oriented two-stage RO model (Case 2)			
		Inner loop iterations	Outer loop iterations	Total time (s)	TotalCost ($)
7	1	2	2	118.00	2,397,426.10
	2	3	3	174.57	914,536.54
	3	3	3	185.19	881,633.36
6	1	2	2	112.31	2,243,992.98
	2	3	3	172.32	823,809.41
	3	4	4	230.47	754,821.73
5	1	2	2	111.93	2,220,605.76
	2	3	3	173.14	693,076.63
	3	4	4	236.92	646,376.79

2) Compared to the traditional resilience-constrained unit commitment, the proposed comprehensive planning-operation framework can not only ensure the power supply for load demand but also reduce the risk of generation curtailment, exhibiting better economic performance. Furthermore, a sensitivity analysis of the proposed model enables the planner to achieve a tradeoff between the robustness of resilience decisions and economic benefits before typhoon attacks. Notably, with the increasing line hardening budgets, the solution efficiency for the model could be sacrificed.

In the future, based on the framework of prevention and emergency response, we will further consider the recovery strategy after typhoon events to improve the DN resilience, such as repair crews and mobile power resources.

CRediT authorship contribution statement

Zhanghao Huang: Conceptualization, Methodology, Software, Visualization, Writing – original draft, Writing – review & editing. **Yachao Zhang:** Supervision, Funding acquisition, Writing – review & editing. **Shiwei Xie:** Writing – review & editing.

Declaration of Competing Interest

The authors declare that they have no known competing financial interests or personal relationships that could have appeared to influence the work reported in this paper.

Data availability

Data will be made available on request.

Acknowledgements

This work was supported by National Natural Science Foundation of China (No. 61903088).

References

[1] Ofpresident EO, Economic benefits of increasing electric grid resilience to weather outages. White house, Tech. Rep. (2013). Jul.
[2] H Gao, Y Chen, S Mei, et al., Resilience-oriented pre-hurricane resource allocation in distribution systems considering electric buses, Proc IEEE 105 (7) (2017) 1214–1233.
[3] Shahinzadeh H, Nikolovski S, Moradi J, et al. A resilience-oriented decision-making model for the operation of smart microgrids subject to techno-economic and security objectives, In: 2021 9th International Conference on Smart Grid, ICSG 2021: 226-230.
[4] KP Schneider, FK Tuffner, MA Elizondo, et al., Evaluating the feasibility to use microgrids as a resiliency resource, IEEE Trans. Smart Grid 8 (2) (2017) 687–696.
[5] S Ma, B Chen, Z. Wang, Resilience enhancement strategy for distribution systems under extreme weather events, IEEE Trans. Smart Grid 9 (2) (2018) 1442–1451.
[6] M Mahzarnia, MP Moghaddam, PT Baboli, et al., A review of the measures to enhance power systems resilience, IEEE Syst. J. 14 (3) (2020) 4059–4070.
[7] X Wang, Z Li, M Shahidehpour, et al., Robust line hardening strategies for improving the resilience of distribution systems with variable renewable resources, IEEE Trans. Sustain. Energy 10 (1) (2019) 386–395.
[8] H Zhang, S Ma, T Ding, et al., Multi-stage multi-zone defender-attack-defender model for optimal resilience strategy with distribution line hardening and energy storage system deployment, IEEE Trans. Smart Grid 12 (2) (2021) 1194–1205.
[9] Y Lin, Z. Bie, Tri-level optimal hardening plan for a resilient distribution system considering reconfiguration and DG islanding, Appl. Energy 210 (2018) 1266–1279.
[10] DK Mishra, MJ Ghadi, A Azizivahed, et al., A review on resilience studies in active distribution systems, Renew. Sustain. Energy Rev. 135 (2021), 110201.
[11] G Huang, J Wang, C Chen, et al., Integration of preventive and emergency responses for power grid resilience enhancement, IEEE Trans. Power Syst. 32 (6) (2017) 4451–4463.
[12] T Ding, Z Wang, W Jia, et al., Multiperiod distribution system restoration with routing repair crews, mobile electric vehicles and soft-open-point networked microgrids, IEEE Trans. Smart Grid 11 (6) (2020) 4795–4808.
[13] Y Wang, L Huang, M Shahidehpour, et al., Resilience-constrained hourly unit commitment in electricity grids, IEEE Trans. Power Syst. 33 (5) (2018) 5604–5614.
[14] T Ding, M Qiu, Z Wang, et al., Power system resilience enhancement in typhoons using a three-stage day-ahead unit commitment, IEEE Trans. Smart Grid 12 (3) (2021) 2153–2164.
[15] C Zhao, R. Jiang, Distributionally robust contingency-constrained unit commitment, IEEE Trans. Power Syst. 33 (1) (2018) 94–102.
[16] General electrics LM6000 series manual. [Online]. Available: https://www.ge.com/power/gas/gas-turbines/lm6000.
[17] MA Gilani, A Kazemi, M. Ghasemi, Distribution system resilience enhancement by microgrid formation considering distributed energy resources, Energy 191 (2020), 166442.
[18] R Wu, G. Sansavini, Integrating reliability and resilience to support the transition from passive distribution grids to islanding microgrids, Appl. Energy 272 (2020), 115254.
[19] A Younesi, H Shayeghi, A Safari, et al., Assessing the resilience of multi microgrid based widespread power systems against natural disasters using Monte Carlo Simulation, Energy 207 (2020), 118220.
[20] DN Trakas, ND. Hatziargyriou, Optimal distribution system operation for enhancing resilience against wildfires, IEEE Trans. Power Syst. 33 (2) (2018) 2260–2271.
[21] B Hu, M Li, T Niu, et al., Hardening planning of overhead distribution lines in typhoon-prone areas by considering the typhoon motion paths and the line load reliability, Int. J. Electr. Power Energy Syst. 129 (5) (2021), 106836.
[22] C Wang, W Wei, J Wang, et al., Robust defense strategy for gas-electric systems against, malicious attack, IEEE Trans. Power Syst. 32 (4) (2016) 2953–2965.
[23] DN Trakas, ND. Hatziargyriou, Resilience constrained day-ahead unit commitment under extreme weather events, IEEE Trans. Power Syst. 35 (2) (2020) 1242–1253.
[24] T Ding, L Yao, F. Li, A multi-uncertainty-set based two-stage robust optimization to defender-attacker-defender model for power system protection, Reliab. Eng. Syst. Saf. 169 (2018) 179–186.
[25] W Yuan, J Wang, F Qiu, et al., Robust Optimization-based resilient distribution network planning against natural disasters, IEEE Trans. Smart Grid 7 (6) (2016) 2817–2826.
[26] C Wang, Y Hou, F Qiu, et al., Resilience enhancement with sequentially proactive operation strategies, IEEE Trans. Power Syst. 32 (4) (2017) 2847–2857.
[27] H Zhang, L Cheng, S Yao, et al., Spatial-temporal reliability and damage assessment of transmission networks under hurricanes, IEEE Trans. Smart Grid 11 (2) (2020) 1044–1054.
[28] M Esfahani, N Amjady, B Bahareh, et al., Robust resiliency-oriented operation of active distribution networks considering windstorms, IEEE Trans. Power Syst. 35 (5) (2020) 3481–3493.
[29] H Wang, J Yan, S Han, et al., Switching strategy of the low wind speed wind turbine based on real-time wind process prediction for the integration of wind power and EVs, Renew. Energy 157 (2020).
[30] M Bao, Y Ding, M Sang, et al., Modeling and evaluating nodal resilience of multi-energy systems under windstorms, Appl. Energy 270 (2020) 115–136.
[31] A Shafieezadeh, UP Onyewuchi, MM Begovic, et al., Age-dependent fragility models of utility wood poles in power distribution network against extreme wind hazards, IEEE Trans. Power Del. 29 (1) (2014) 131–139.
[32] S Bjarnadottir, Y Li, MG. Stewart, Hurricane risk assessment of power distribution poles considering impacts of a changing climate, J. Infrastruct. Syst. 19 (1) (2012) 12–24.
[33] W Yuan, J Wang, F Qiu, et al., Robust Optimization-based resilient distributionnetwork planning against natural disasters, IEEE Trans. Smart Grid 7 (6) (2016) 2817–2826.
[34] T Ding, Y Lin, G Li, et al., A new model for resilient distribution systems by microgrids formation, IEEE Trans. Power Syst. 32 (5) (2017) 4145–4147.
[35] H Gao, J Liu, L Wang, et al., Robust coordinated optimization on active and reactive power in active distribution systems, IEEE Trans. Smart Grid 7 (1) (2016) 301–311.
[36] ME Baran, FF. Wu, Network reconfiguration in distribution systems for loss reduction and load balancing, IEEE Trans. Power Del. 4 (2) (1989) 1401–1407.
[37] Typhoon Path, 2022. [Online]. Availale: http://typhoon.nmc.cn/web.html.